Chapter 11

Optical on–off keying data links for low Earth orbit downlink applications

Dirk Giggenbach[1], Florian Moll[1], Christopher Schmidt[1], Christian Fuchs[1], and Amita Shrestha[1]

Optical free-space links will shape the high-speed communications technology landscape for space missions substantially in the next years. The dramatically reduced signal spread – as compared to any radio frequency (RF) technology – provides a variety of advantages: increased power efficiency, the avoidance of interference and thus spectrum regulation issues, the inherent tap- and spoof-proofness and, most of all, the vastly increased data rates (DRs) will make this technology a 'game changer' comparable to the introduction of glass fibre instead of copper cables previously used in the global communication infrastructure.

As one use case of optical space links high-speed geostationary data-relays for the repatriation of low Earth orbit (LEO) observation satellite telemetry have been tested and are currently implemented operationally by various space agencies [1–4]. Deep space missions will also boost their DRs by several orders of magnitude by sending their data to large optical receiver telescopes, NASA is currently transforming its Deep Space Network to an optical DNS, and we also see European developments in optical deep space communications [5–7]. In order to connect very high-throughput communication satellite systems to the Tbps-regime (Terabit-per-second), optical uplinks can solve the spectrum bottleneck that RF links would otherwise encounter [8]. In the LEO regime (inter-satellite, as well as optical LEO downlinks – OLEODL), distances are way shorter, allowing very high data rates while, at the same time, reducing the requirement for high system sensitivity (where complexity and thus costs generally increase with sensitivity). Instead, components and technologies that are close to commercial-off-the-shelf (COTS) from terrestrial fibre communications can be used, allowing both very high throughputs and moderate-to-low system costs. Using COTS components in inter-satellite as well as downlinks is also supported by the shorter life time of LEO missions, implying less radiation exposure of these components. In the last years, several demonstrations of OLEODL have been performed by various agencies [9–15], and its commercialisation will be seen in near future.

[1] Satellite Networks Department, German Aerospace Center, Institute of Communications and Navigation, Germany

OLEODL serve for sensor data download from earth observation satellites, their link scenario is strongly asymmetric, since the data flow is mostly simplex or at least the downlink DR is orders of magnitude higher than the uplink (the later may only serve for tele-command and link protection). Therefore, the antenna gain can be distributed favourably: with small and lightweight transmitters in space and correspondingly moderately sized antennas (i.e., receiver telescope apertures) on the ground. The disturbing atmosphere only affects the lower end of the link close to the receiving ground station, which on the one hand allows for simple techniques for link stabilisation by aperture averaging but on the other hand complicates some of the advanced modulation and detection formats, since these may require sophisticated techniques like adaptive optics for coupling into single-mode fibres. Therefore, data format options for OLEODL focus mainly on rather low complex and robust direct detection (DD) techniques [16].

The following chapter introduces in its subsections:

- the implementation history of space terminals and optical ground stations (OGSs) and consequences of the link scenario geometry
- effects of the atmospheric transmission channel, link budget, modulation formats and link protection techniques
- system and component aspects, and an outlook to ongoing and future missions and systems.

11.1 The scenario and history of optical LEO data downlinks

11.1.1 Optical LEO downlink experiments overview

OLEODL – in contrast to their traditional RF counterparts – enable higher data throughput from earth observation satellites while avoiding spectrum regulation issues. This has attracted attention for several decades now and has resulted in multiple experimental or demonstration space missions, see Figure 11.1. One of the first were the downlink campaigns from the Japanese satellite Kirari (also named *OICETS*) to ground stations in Japan, Europe and the United States in 2006 and 2009 [17,18]. While this mission was compatible with the European geostationary Earth orbit (GEO)-relay terminals of semi-conductor inter-satellite link experiment [19] and thus used wavelengths in the semi-conductor laser domain, later on the OLEODL projects focused on 15xx nm as the carrier wavelength since this allows to build on component technology from terrestrial fibre communications like optical amplifiers and laser diodes. Furthermore, eye safety can be achieved more easily and solar background radiation causes less disturbance at longer wavelengths. These follow-on projects comprise SOTA by NICT (Small Optical Transponder, on-board SOCRATES Satellite) [20], OPALS (Optical Payload for Lasercomm Science, on-board the ISS) by the Jet Propulsion Lab (JPL) and the various development stages of DLR's OSIRIS (Optical Space InfraRed link System) [21]. Chinese and Russian experiments have also been reported. OLEODLs were also performed from the LCTs

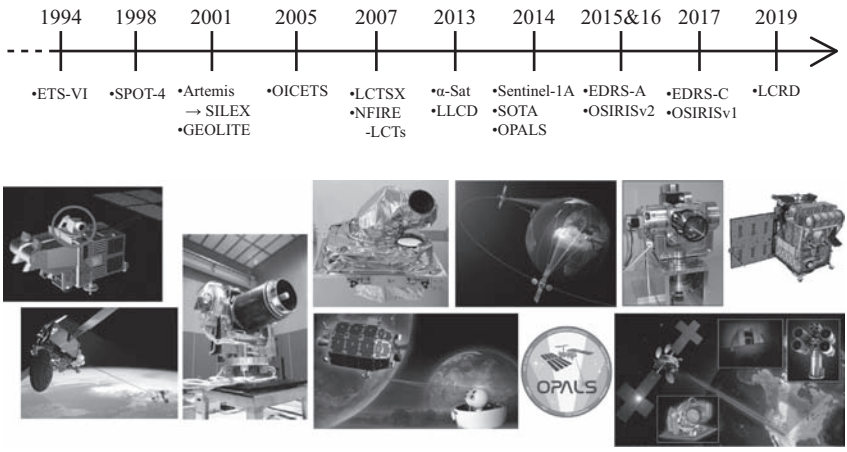

Figure 11.1 Recent timeline of space laser missions. Pictures: ESA, NASA, JAXA, NICT, DLR

on-board TerraSAR-X, testing sensitive and elaborate coherent BPSK-homodyne modulation [22]. Table 11.1 provides an overview of some project parameters.

Several institutions operate OGSs in order to carry out such downlink experiments not only from LEO but also from GEO and farther space probes. OGSs on Tenerife, in California and in Tokyo, have been established since the 1990s [23–26]. Newer – partly temporary – sites include Hawaii, White Sands in New Mexico, Oberpfaffenhofen near Munich, Observatoire de la Côte d'Azur (OCA) [27] and several more stations in Japan like Okinawa and Kashima. Other institutions also operate astronomical facilities in temporary use as ground stations in optical communication experiments. Table 11.2 illustrates the basic parameters of some OGS installations.

In the future, further developments in the domain of OLEODL are expected in Japan (VSOTA on RISESAT), Europe (OSIRIS-v3 [28], OPTEL-μ [29]) and the United States [30]. Standardisation efforts are ongoing in the *Consultative Committee for Space Data Systems* (CCSDS) to advance global cooperation in this domain [31].

11.1.2 Performance and geometrical restrictions

An OLEODL link includes the downlink signal from the satellite which is detected and tracked at the ground station telescope, and an uplink beacon signal from the ground station to the satellite which allows the space terminal precise tracking of the OGS location during the overflight. Optical links, just as any traditional RF LEO downlinks, encounter the same geometrical conditions here as depicted in Figure 11.2 and summarised in Table 11.3. A typical low altitude for Earth observation satellites is 400 km, whereas 900 km is typical for a satellite communication network. An optical downlink should generally start acquisition of the optical signals at around 5° elevation, and secure data transmission should work from 10° elevation upwards.

Table 11.1 Overview of optical LEO downlink projects (selection)

Optical terminal	**LUCE**	**LCTSX**	**SOTA**	**OPALS**	**OSIRIS v2**	**OSIRIS v1**	**OSIRIS v3**
Operator	JAXA	DLR	NICT	JPL	DLR	DLR	DLR
In orbit	2005	2006	2014	2014	2016	2017	2019
Satellite or platform	**OICETS/ Kirari**	**TerraSAR-X**	**SOCRATES**	**ISS**	**BIROS**	**Flying Laptop**	**TBC**
Orbit height (circular)	~600 km	515 km	600 km	~400 km	510 km	600 km	TBC
CPA type	az-el	periscope	az-el	az-el	Sat-Pointing w. 4QT	Sat-Point. open-loop	1-mirror
Tx wavelength	847 nm	1,064 nm	1,549 nm	1,550 nm	1,545 and 1,550 nm	1,550 nm	1,540 nm
Tx power (typical, mean)	0.1 W	0.7 W	35 mW	0.8 W	0.5 and 0.05 W	0.5 W	1 W
Tx divergence (FWHM)	5.5 μrad	–	223 μrad	940 μrad	200 and 1,200 μrad	200 μrad	TBC
Data rate, channel	50 Mbps	5.6 Gbps	1/10 Mbps	50 Mbps	1 Gbps	10/100 Mbps	10 Gbps
Uplink/beacon wavelength	820 nm	1,064 nm	1,064 nm	976 nm	1,560 nm	N.A.	1,590 nm
Uplink data rate	2 Mbps	5.6 Gbps	N.A.	N.A.	100 kbps	N.A.	TBD
Downlinks to OGSs	NICT-Tokyo OGS-OP ESA-Tenerife JPL-TMF	ESA-OGS OGS-OP Calar-Alto	NICT-Tokyo NICT–other OGS OGS-OP/TOGS CSA CNES-OCA	OCTL (TMF) OGS-OP/TOGS	OGS-OP/TOGS	OGS-OP/TOGS	OGS-OP/ TOGS–future
Mission status (Jan 2018)	Finished	Finished	Finished	Finished	Launched	Launched	In development

Table 11.2 Global installations of optical ground stations for OLEODL signal reception (selection)

OGS	Tenerife-Izana, Spain (ESA-OGS)	Tokyo–Koganei, Japan	Table Mountain, CA, USA (OCTL)	Oberpfaffenhofen, Germany (OGS-OP)	Worldwide (TOGS)
Operator	ESA	NICT	JPL-NASA	DLR	DLR
Operational since	1997	1994	2003	2006	2010
Location a.s.l.	2,400 m	70 m	2,288 m	600 m	Portable
Rx aperture diameter	100 cm	100 and 150 cm	100 cm	40 cm	60 cm
Telescope and mount type	Cassegrain and Coudé	Nasmyth and Coudé	Az.-El., Coudé	Cassegrain and Coudé	Ritchey Chretien
Employed in links from	OPALE (on Artemis) LUCE (on OICETS) LCTSX (on TerraSar-X) SOTA (on SOCRATES) OPALS (on ISS) LLCD (on LADEE)	ETS-VI LUCE SOTA	LUCE LLCD OPALS	LUCE OPALS SOTA OSIRIS	SOTA OSIRIS VABENE

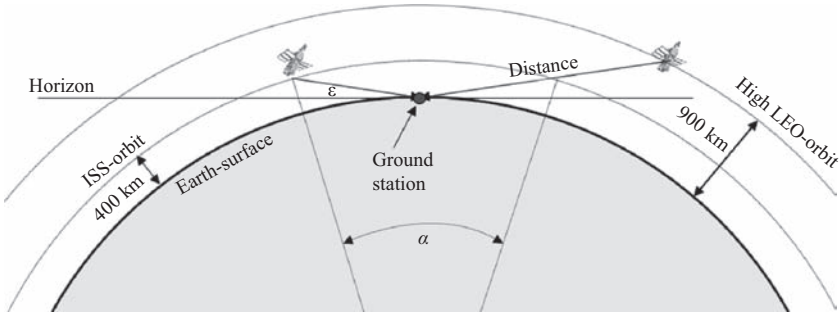

Figure 11.2 Link geometry of typical LEO satellite downlinks with circular orbits

Table 11.3 Parameters for the two satellite altitudes depicted in Figure 11.2. Absolute velocity and thus also the point-ahead angle of both orbits are nearly the same; however, their visibility time, distance, and maximum slew rate differ by ca. factor of two.

Orbit altitude (km)	**Distance at 5° (km)**	**Max. link duration 5°→5° (s)**	**Angular slew rate at zenith (°/s)**	**Point-ahead at zenith (μrad)**
400	1,804	475	1.1	51
900	2,992	831	0.48	49

A key parameter is the point-ahead angle (PAA) of the uplink versus the downlink direction, which originates from the fast orthogonal velocity of the satellite versus the ground station (the satellite moves several metres during the time of flight of the signals). Since optical signal divergence angles are small, they can be in the same order as this PAA, and as a result, the PAA offset must be taken into account for the alignment of the opto-mechanical systems.

When the LEO satellite is in the line of sight of an OGS, its viewing elevation is restricted to low elevations most of the time, as the simulation result in Figure 11.3 depicts for 500 km orbit height. When defining 5° as the minimum possible contact elevation, the satellite is seen between 5 and 20° for 64% of the total contact time. This has a major influence on the data format and link protection, since higher range loss is experienced at lower elevations and atmospheric disturbances have a greater impact.

11.1.2.1 Throughput advantage and spectrum issues

Optical link technology currently uses only one wavelength to achieve transmission rates of several Gbps; however, from terrestrial fibre communications, we see how this rate can increase into the Tbps-regime by multiple channels (dense wavelength

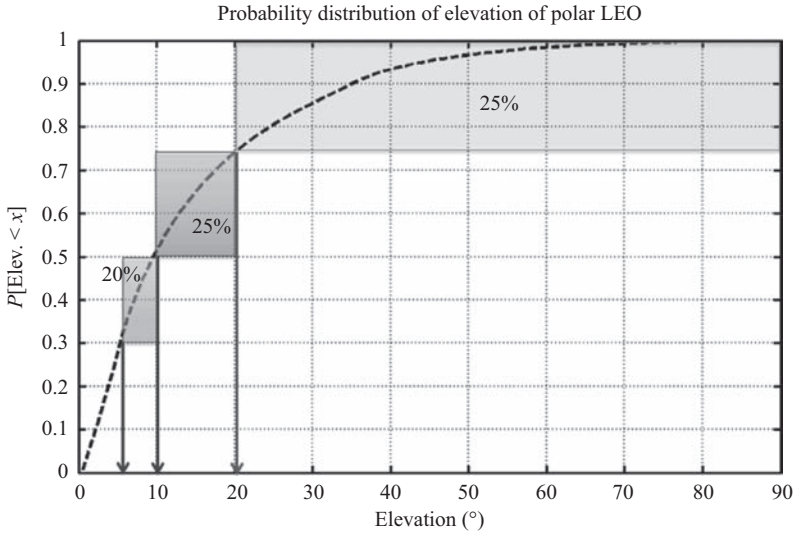

Figure 11.3 Typical distribution of the average viewing elevation for a polar LEO satellite (500 km orbit height). This relative distribution is qualitatively similar for any OGS location on earth, although of course the absolute overall visibility changes depending on orbit and OGS latitude [32]

division multiplexing) and higher order modulation formats. From available channel capacity, optical links offer several Terahertz of spectrum and thus according combined DRs, while RF links will always be strongly limited in spectrum and thus throughput. See [33] for an estimation of OLEODL system throughput taking into account realistic cloud blockage statistics.

Another motivation to move directly to optical links in LEO downlinks and avoid other higher frequency RF techniques is to avoid spectrum interference issues with future 5G mobile communications standards which are moving into the millimetre wave domain.

11.1.3 Data rates and rate change for a variable link budget

Targeted DRs in OLEODL range from a few megabits per second for very simple and low-cost satellites and terminals with limited pointing control and transmit power, to several gigabits per second for high throughput Earth observation sensor data downloads. Since the corresponding OGSs should not require adaptive optics for single mode fibre coupling in the first place, an upper channel rate limit of at least 10 Gbps is assumed – a rate at which multi-mode photo detectors can still be used. An optimised data throughput does, however, not only depend on the maximum possible DR, but also on the variation of the rate due to link constraints such as channel attenuation and

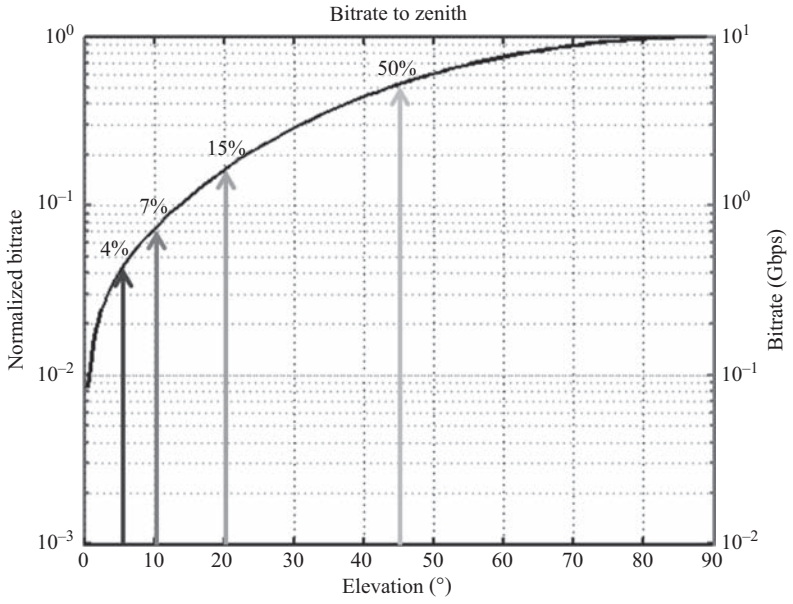

Figure 11.4 Downlink bitrate normalised to zenith, for constant energy per bit (i.e. sensitivity per bit is independent of data rate), including range and atmospheric losses

power variation as caused by the index-of-refraction turbulence (IRT) of the atmosphere. These two effects – varying link budget due to distance and atmospheric attenuation, and fast power scintillation due to atmospheric IRT – are the key challenges in OLEODL. The effect of atmospheric scintillation has been investigated in depth by various publications [34] and shall not be detailed in this text.

Directly connected to the link elevation is the maximum achievable DR. Assuming a receiver that performs with constant energy/bit, a link from 5° elevation to zenith allows a rate variation of around 25, as Figure 11.4 depicts. This plot includes the elevation-dependent atmospheric signal attenuation, but not the dynamic scintillation and fading effects caused by atmospheric turbulence, which will be explained later in this chapter. However, such an ideal receiver and the corresponding transmitter (one that can change its rate continuously) do not exist in practice. Therefore, few hard DR steps must be assumed or even just one fixed rate. The total throughput with a fixed rate would, even at best, be only one-third of the ideal maximum throughput with a continuously variable rate [35].

While the foregoing exemplification implies that the source DR equals the channel symbol rate, generally this is not the case since further mechanisms influence their relation (generally symbol rate is higher than DR), of which some are shown in Figure 11.5.

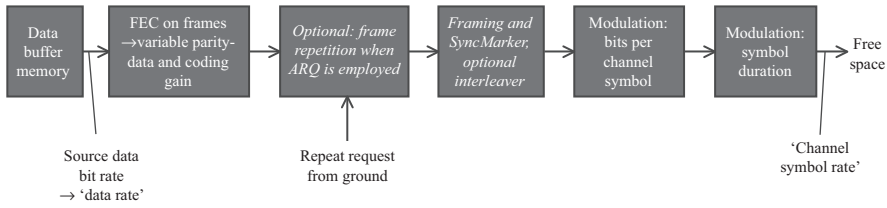

Figure 11.5 Steps in the transmitter data processing chain of the optical space terminal

FEC (forward error correction) is the standard technique used to protect data against bit errors in a simplex link, and its ratio of coding overhead versus total data payload, together with the according FEC-gain variation, allows for some rate variability. Automatic Repeat Request (ARQ) is an alternative – or additional – link protection mechanism, which, however, requires a return channel (uplink) which cannot be ensured. Other optional methods, such as burst transmission with pauses between data sections, frame repetition and inter-leaver techniques, partly proof advantageous in a fading channel. The variation of bits per channel symbol with on–off-Keying (OOK) modulation is, e.g. done with a pulse position modulation (PPM) or Amplitude-Shift-Keying modulation format, where one pulse transmits the information of more than one bit. Finally, the simplest way to vary the effective DR is to alter the length of one symbol time.

These mechanisms are used in different sophistication levels of rate variation modes, in order to maximise the overall downlink system throughput under varying link loss, while also securing a frequent access to the satellite. Note that variations in the effective source DR do not necessarily require a change in channel symbol rate.

Different modes of varying the DR in an OLEODL-system can be identified:

1. While a specific satellite terminal might only work at one DR, still an OGS may need to vary its Rx rate since it serves different types of satellite missions.
2. A constant rate during one downlink contact is chosen according to its pass geometry, e.g. to allow maximum throughput during this link.
3. Depending on the progression of the link elevation, the transmitter varies the effective DR on pre-programmed time steps, to adopt to the known elevation-dependent link losses.
4. By exchanging channel state information between ground and satellite, the optimum rate is chosen dynamically, every time the link budget changes notably.

11.2 Link design

The basis for any system development is the preceding link design. In our approach, this comprises analysis of the propagation channel, definition of the transmission equation, calculation of the link budget, consideration of the pointing, acquisition

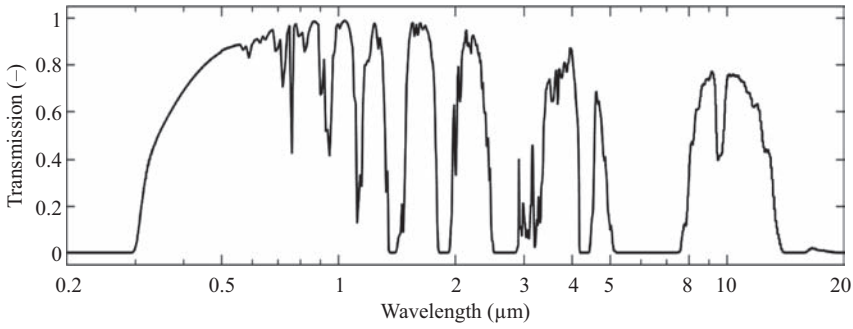

Figure 11.6 Clear sky atmospheric transmission spectrum from sea level to space in zenith direction, from 200 nm to 20 μm calculated with libRadtran using the LOWTRAN model. The transmission is the ratio I_{out}/I_{in} from (11.1) [36]

and tracking (PAT) process, modulation formats, receiver technology and impact of bit coding and higher layer coding and protocols.

11.2.1 Propagation channel model

With respect to propagation characterisation, we distinguish between two groups of effects: extinction of the atmosphere and turbulence effects. Extinction means a loss of energy of the propagating electro-magnetic wave by absorption and scattering processes. Presuming that the extinction is not dependent on the intensity of the wave, it can be described by Beer's law. It models the attenuation of a propagation path through a medium with an exponential law using the medium specific extinction coefficient $\alpha_{\text{ext}}(\lambda)$ (km^{-1}) and path length L (km), assuming a homogeneous medium and monochromatic light. Let I_{in} (W/m^2) be the input intensity to the medium and I_{out} (W/m^2) the output intensity, then

$$I_{\text{out}} = I_{\text{in}} \cdot \exp(-\alpha_{\text{ext}}(\lambda) \cdot L). \tag{11.1}$$

For the case of a non-homogeneous medium, the argument of the exponential function is defined by an integral over the path length.

The wavelength dependency of the extinction determines the atmospheric transmission spectrum. A calculation of the spectrum between 200 nm and 50 μm is given in Figure 11.6 (based on a clear sky atmosphere). The atmospheric windows are clearly visible.

While Figure 11.6 identifies the large spectral atmospheric transmission windows, when looking in detail at the situation around specific wavelengths and consider low link elevations, thin molecular absorption lines can become dominant. These lines are mostly produced by water vapour and carbon dioxide molecules and have a typical width of a few GHz, while their occurrence is roughly two lines per nm. As elucidated in Figure 11.7 (with atmospheric model *mid-latitude-summer*,

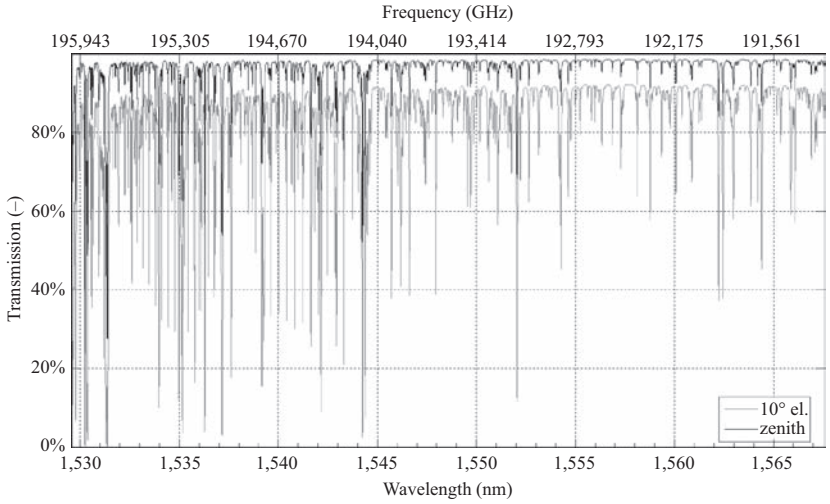

Figure 11.7 Molecular absorption lines mostly due to water vapour impact the atmospheric transmission in C-band (1,530–1,565 nm), especially at low link elevations. Simulated using the atmospheric constituent profiles and absorption coefficients derived from the HITRAN database [37]

continental-clean aerosol model and *volcanic activity two* out of four), it becomes obvious that for typical OLEODL elevations, the lower part of the commonly used C-band shows more of these absorption lines than the upper part. While the water content of the atmosphere reduces with altitude and thus ground stations on mountain tops will be less affected by these absorption effects, one must not limit the applicability of OLEODL technology to OGSs at favourable geographical locations. Rather, careful wavelength selection and stability control of up- and downlink sources can ensure reliable operation to any OGS site.

The second group of atmospheric effects relates to IRT. These effects cause phase distortions during propagation of the electro-magnetic wave from space to ground. The distorted phase front causes constructive and destructive self-interference of the wave which results in a stochastic intensity pattern of the beam changing spatially and temporally, called intensity scintillation. A variety of phase and intensity effects are created by the process of IRT which are isolated for the sake of easier modelling. The strength is governed by the strength of the turbulence, the length of the propagation path and, in the case of a slant path, the direction of propagation. Table 11.4 lists the most important effects.

These effects are usually modelled by means of a statistical description. Furthermore, different scenarios are categorised according to their fluctuation regime, which is used to select the appropriate model for the statistical description: weak, moderate and strong.

Table 11.4 Overview of effects on laser beam due to atmospheric turbulence

Effect	Type	Description
Wavefront distortions	Phase	Distortion of the spatial two dimensional wavefront
Beam tilt	Phase	Change of propagation direction as seen from the source
Angle of arrival fluctuations	Phase	Change of propagation direction as seen from the receiver
Intensity scintillation	Intensity	Spatial and temporal fluctuation of intensity
Beam broadening	Intensity	Causes increase of beam waist

11.2.2 Transmission equation

The transmission equation describes the link at the system level and is used to calculate the link budget for specific system designs. One particular form of the transmission equation which is suitable for optical satellite links and described in [38] reads

$$P_\mathrm{r} = P_\mathrm{t}\tau_\mathrm{t}G_\mathrm{t}L_\mathrm{fs}G_\mathrm{r}\tau_\mathrm{r}\tau_\mathrm{rp} \tag{11.2}$$

with P_r (W) being the received optical power, P_t (W) the average optical transmit power, τ_t [–] the optical loss in the transmitter, G_t [–] the transmit antenna gain, L_fs [–] the free-space loss, G_r [–] the receive antenna gain, τ_r [–] the optical loss in the receiver and τ_rp [–] the pointing loss of the receiver.

This equation does not contain the pointing loss of the transmitter τ_tp [–], the atmospheric extinction loss τ_ext [–], the atmospheric turbulence loss τ_turb [–], the loss due to background light τ_bgl [–] and coding gain G_c [–]. The extended transmission equation is

$$P_\mathrm{r} = P_\mathrm{t}\tau_\mathrm{t}G_\mathrm{t}\tau_\mathrm{tp}L_\mathrm{fs}\tau_\mathrm{ext}\tau_\mathrm{turb}\tau_\mathrm{rp}\tau_\mathrm{bgl}G_\mathrm{r}G_\mathrm{c}\tau_\mathrm{r} \tag{11.3}$$

which is valid assuming independence of the individual loss and gain effects.

The peak antenna transmit gain in the case of a homogeneous intensity distribution is expressed by

$$G_\mathrm{t} = \frac{16}{\theta_\mathrm{div}^2} \tag{11.4}$$

with θ_div (rad) being the full divergence angle. It must be noted that the denominator in (11.4) is set to 32 in the case of a Gaussian intensity distribution since its peak is twice its mean intensity. The free-space loss is given by

$$L_\mathrm{fs} = \left(\frac{\lambda}{4\pi z}\right)^2 \tag{11.5}$$

with the wavelength λ (m) and the propagation path length z (m). The receiving antenna gain is

$$G_\mathrm{r} = \left(\frac{2\pi r_\mathrm{Rx}}{\lambda}\right)^2 \tag{11.6}$$

with the radius of the receiving antenna r_Rx (m).

The extinction loss is defined by Beer's law [Equation (11.7)].

$$\tau_{\text{ext}} = \frac{I_{\text{in}}}{I_{\text{out}}}. \tag{11.7}$$

The loss due to background light τ_{bgl} [–] for incoherent systems can be written as

$$\tau_{\text{bgl}} = f(R_{\text{atm}}, \Delta\lambda_{\text{bp}}, r_{\text{Rx}}, \theta_{\text{Rx}}, P_{\text{Rx}}) \tag{11.8}$$

with the atmospheric radiance R_{atm} (W/m^2/nm/sr), the optical bandpass bandwidth $\Delta\lambda_{\text{bp}}$ (m) and the detector field of view θ_{Rx} (rad). The formalism is kept quite generic here since the background light loss strongly depends on the specific modulation and detection scheme. For a detailed analysis of background light loss, [39] can be consulted, for example, which contains a model for SNR degradation due to background light with a DD receiver using avalanche photo-diode (APD).

The optical losses in the transmitter and receiver depend on the material characteristics of the actual implementation, mainly on the quality of the anti-reflection and reflection coatings. Furthermore, a fraction of the energy may be split from the communication system to the PAT sensors, which is also considered an optical loss here. The losses due to miss-pointing of the transmitter and receiver are statistical losses and depend on the miss-pointing bias of the transmitter $\theta_{\text{tp,bias}}$ (rad), the miss-pointing jitter of the transmitter $\sigma_{\text{tp,jit}}$ (rad), the miss-pointing bias of the receiver $\theta_{\text{rp,bias}}$ (rad), the miss-pointing jitter of the receiver $\sigma_{\text{rp,jit}}$ (rad) and the probability p_{thr} [–] of the received signal dropping below a defined threshold F_{thr} (dB).

$$\tau_{\text{tp}} = f(\sigma_{\text{tp,jit}}, \theta_{\text{tp,bias}}, p_{\text{thr}}, F_{\text{thr}}) \tag{11.9}$$

and

$$\tau_{\text{rp}} = f(\sigma_{\text{rp,jit}}, \theta_{\text{rp,bias}}, p_{\text{thr}}, F_{\text{thr}}). \tag{11.10}$$

IRT of the air cause spatial and temporal intensity fluctuations which lead to fades and surges (scintillation) in the received power with millisecond timescale. The according dynamic signal quality loss depends on the specific transmission system and is defined similar to the pointing losses, i.e. it is a dynamic loss expressed through statistical parameters. The turbulence loss can be written in the very generic form as

$$\tau_{\text{turb}} = f(w_0, C_{\text{n}}^2(z), r_{\text{Rx}}, p_{\text{thr}}, F_{\text{thr}}). \tag{11.11}$$

This includes modelling of the turbulence channel with the path profile of the index of refraction constant $C_{\text{n}}^2(z)$ (m$^{-2/3}$) which describes the strength of the turbulence along the propagation path. In the special case of an incoherent system with OOK and DD, and assuming a turbulent channel with lognormal power fluctuation statistics, Giggenbach and Henniger [40] developed a model to assess turbulence loss for lognormal power distribution and a fixed loss threshold p_{thr}

$$\tau_{\text{turb}} = \frac{\exp\left\{\text{erf}^{-1}(2p_{\text{thr}} - 1)\left[2\ln\left(\sigma_{\text{p}}^2 + 1\right)\right]^{1/2}\right\}}{\left(\sigma_{\text{p}}^2 + 1\right)^{1/2}}. \tag{11.12}$$

The power scintillation index σ_{p}^2 [–] covers the profile of the index of refraction structure parameter and the size of the receiver aperture.

The coding gain G_c [–] is defined according to [41] by

$$G_c = \frac{P_{\text{min,uncoded}}}{P_{\text{min,coded}}} \tag{11.13}$$

where $P_{\text{min,uncoded}}$ (W) is the necessary minimum power in the event that no coding is applied for a given target bit error rate BER_{tg} [–], and $P_{\text{min,coded}}$ (W) is the necessary minimum power in the event that a particular coding is applied. In the case of an atmospheric turbulent channel, the dependencies of the coding gain on channel parameters can be expressed with

$$G_c = f(\sigma_P^2, \tau_{p,corr}, \sigma_N^2, BER_{tg}) \tag{11.14}$$

where $\tau_{p,corr}$ (s) is the correlation time of the received power defined via the autocovariance function. Lognormal statistics of received power are once again assumed. The use of $\tau_{p,corr}$ assumes that the spectral shape of the fluctuations is known. However, since this is not necessarily the case, (11.14) may contain the power spectrum of the fluctuations $S_{scint}(f)$ instead of the correlation time. The parameter σ_N^2 denotes additional electrical noise.

11.2.3 Link budget

Based on the extended transmission equation (11.3), power budgets of the link can be calculated. It is customary to write the parameters of the link equation in dB and to present the link budget in a table. The influence of each parameter can thus easily be identified. In the following, we present example link budgets for satellite-to-ground downlinks as well as the beacon uplink.

We chose a satellite in a typical Earth observation orbit with an altitude of about 700 km. This results in a link distance of about 2,100 km at an elevation angle of 10°, which is considered the start elevation for the communication link, and about 2,500 km at an elevation angle of 5°, which is considered as start elevation for link acquisition. A wavelength of 1,550 nm is used as it is most common for OLEODL today.

Table 11.5 shows the resulting link budgets for downlink and uplink. Please note that several of the previously defined parameters are given in dB here. Satellite-to-ground links for Earth observation applications, in particular, can be designed highly asymmetric. A high throughput is only required to transmit mission data back to Earth, while a low-rate uplink is sufficient, e.g. for the exchange of channel status information. This allows for a small terminal in space – in the given example, a receiver aperture of only 25 mm is used for the satellite terminal.

Typical values of the downlink laser communication chain are assumed. The transmitter divergence angle is set to 100 μrad, receiver telescope size to 60 cm in diameter and transmit power is 1 W. The data rate is set to 10 Gbps, which results in a required Rx power of −29 dBm, assuming that the sensitivity of a state-of-the-art receiver front end (RFE) with an APD is about 1,000 Ph/bit at a BER of 1E–6, as a conservative value (better can be achieved in practice). The values for pointing loss, turbulence loss, extinction loss and background light loss are selected based on typical implementations. The coding gain is chosen as an example of a standard Reed–Solomon FEC implementation. When experiencing strong scintillation (e.g. when

Table 11.5 Example link budgets for data downlinks at 10 Gbps and beacon uplinks for tracking and tele-command, for a typical Earth observation satellite at 10° elevation, and the beacon at 5° elevation to start acquisition

Parameter	Unit	Data-downlink	Data-uplink	Beacon-uplink (5°)
P_t	dBm	30	40	40
τ_t	dB	−1.5	−1	−1
G_t	dB	92.0	78.1	78.1
τ_{tp}	dB	−3	−3	−3
L_{fs}	dB	−264.6	−264.6	−266.1
τ_{ext}	dB	−4	−4	−8
τ_{turb}	dB	−5	−5	−3
τ_{rp}	dB	−1	−1	0
τ_{bgl}	dB	−1	−1	−1
G_r	dB	127.7	100.1	100.1
G_c	dB	4	4	0
τ_r	dB	−2.5	−4.5	−4.5
$\boldsymbol{P_r}$	**dBm**	**−28.9**	**−61.9**	**−68.4**
$\boldsymbol{P_{req}}$	**dBm**	**−29**	**−69**	**−70**
Margin	**dB**	**+0.1**	**+7.1**	**+1.6**

Note: Bold values of the last three lines indicate the RESULT of the link budget calculation.

the receive aperture is small compared to scintillation pattern), standard interleaving techniques must be employed as mentioned below. Due to the high Rx-power required for 10 Gbps of data rate, the power split for the tracking sensor at the OGS is not critical and therefore not shown here.

A likewise approach has been taken with regard to the uplink direction; however, several parameters differ. For instance, a larger beam divergence is used in order to relax the requirement of OGS pointing and satellite orbit knowledge. Also, a larger Tx power can be used in uplink direction, since no strict power-efficiency limitations are apparent for the OGS. Again, typical values are chosen for the sensitivity of the data-receiver (1,000 Ph/bit for BER $= 10^{-6}$) and the tracking sensor (−70 dBm), which is a typical value to reach the required electrical SNR. Two laser beacons with 5W each are used to take advantage of transmitter diversity to reduce uplink beacon power variation. Eye-safety can be maintained at 1,550 nm even with such high powers when using moderately sized beacon collimators. It is assumed that the same laser is used for tracking (beacon-uplink) and data transmission (data-uplink) of a low-rate uplink with a rate of 1 Mbps that can be used for tele-command purposes or updates of on-board firmware.

It can be observed that in downlink direction, the link margin is small at the given DR of 10 Gbps. As the link shall be operated also at low elevation angles to maximise data throughput of any given mission, it becomes clear that scenarios with a high-link dynamic can benefit substantially from variable data rate techniques, since these allow a rate reduction at low elevation angles and thus a maximisation of the system throughput and link availability.

11.2.4 Pointing, acquisition and tracking

The process of PAT addresses the opto-mechanical system of a laser communication terminal. It is of high importance for any aerospace laser link to obtain line of sight. The first step, **pointing**, relates to the transmit beam steering towards the counter terminal based on a priori information of the position of the partner. In the case of a satellite link, this would be orbit data of the satellite and GPS location data of the ground station, for instance. Depending on the accuracy of the a priori data and the accuracy of the opto-mechanical system (gimbal accuracy, jitter, reference calibration [41]), an angular uncertainty area can be defined where the partner is expected to show up. If this uncertainty area exceeds the transmit beam cone, scanning algorithms must be applied. In the next step, **acquisition**, the beam is detected by the counter terminal using an acquisition sensor, and a control mechanism is activated that steers the beam into the tracking sensor's field of view. Finally, the **tracking** starts. The beam displacement measurement by the tracking sensor continuously creates an error signal used by the control loop to maintain the link lock.

The PAT process often uses a two-stage opto-mechanical system. A course pointing assembly (CPA) defines the field of regard of the satellite or ground terminal and corrects for low frequency, high amplitude bias and jitter. The opto-mechanical implementation is often a two-axes motorised lens/mirror system in combination with a static optical bench similar to a Coudé-path. Alternatively, turret systems that carry the entire electro-optical system are also an option. The precision of the CPA must be high enough to steer the beam into the field of regard of the fine pointing assembly (FPA). This subsystem corrects for high frequency, low amplitude bias and jitter. The sensor is often a four-quadrant diode, and the actuator a voice coil or piezo-driven mirror. For operation during day and night time, it is recommended to use modulated beacon lasers which enable the space segment to discriminate between the beacon laser and background light or earth albedo.

A block diagram for a ground segment that also shows the implemented PAT subsystem is shown in chapter 11.3. The PAT process is illustrated in Figure 11.8 for an exemplary LEO downlink system. The process comprises five steps. In step 1, the ground terminal illuminates the satellite with a high divergence beacon laser. The satellite acquires the signal and corrects its attitude in step 2. In step 3, the satellite points the transmit communications beam to the ground station. In step 4, the ground station acquires the satellite signal using it as a tracking beacon and corrects its pointing direction accordingly, thus both partners obtain line of sight. In step 5, communication is performed and line of sight is maintained via optical tracking.

11.2.5 Direct detection modulation formats and rate variation

Modulation formats considered for OLEODL are mostly based on OOK of the laser signal to encode the bit stream. Detection of such modulation is not hindered by atmospheric wave-front distortions and basically only requires power-in-the-bucket receiver technology which is offered by bulk APD receivers (Avalanche Photo Diodes). Still, if required for higher sensitivity or DRs, more sophisticated techniques, such as pre-amplification in conjunction with fibre coupling and adaptive optics, can be used.

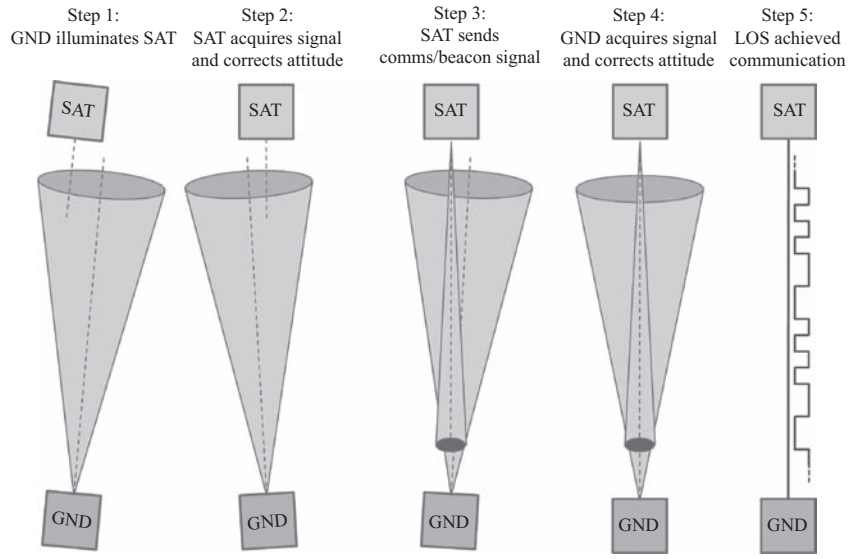

Figure 11.8 PAT process for LEO downlink: the cones qualitatively denote the laser beam divergence; the dashed line represents the optical axis of satellite and ground station

The overall process is therefore also called intensity modulation with DD (IM/DD). The phase of the optical signal does not contain any information, and thus deterioration of the phase does not degrade transmission sensitivity. However, sensitivities similar to coherent phase modulation can be achieved by IM/DD if the appropriate detection technology is used (theoretically 20 photons per on-bit for BER $= 10^{-9}$ when assuming Poisson noise statistics for photon arrival, versus 9 photons per any bit for coherent homodyne BPSK). Such OOK sensitivities could be achieved using the promising technology of single photon detection with superconducting nanowire detectors [42], while today's lower cost APDs reach sensitivities of a few hundred photons per bit and below. Different symbol-encoding schemes can also be applied with OOK, as described in the following, where we outline the most common waveforms.

OOK modulation can be considered the simplest modulation technique in which the intensity of an optical source is directly modulated by the information bit sequence. A bit '1' is represented by an optical pulse while a bit '0' is represented by the absence of an optical pulse. If the pulse occupies the whole bit duration, it is called Non-Return to-Zero (NRZ) OOK, and if the pulse occupies part of the bit duration depending on the duty cycle of the signal, it is called Return-to-Zero (RZ) modulation.

PPM is an orthogonal OOK modulation technique where information is encoded in the time slot when a pulse is transmitted [43]. It is more power efficient in comparison to NRZ and RZ but requires higher bandwidth, and additional complexity requirements must be met during synchronisation and post-processing. In M-ary

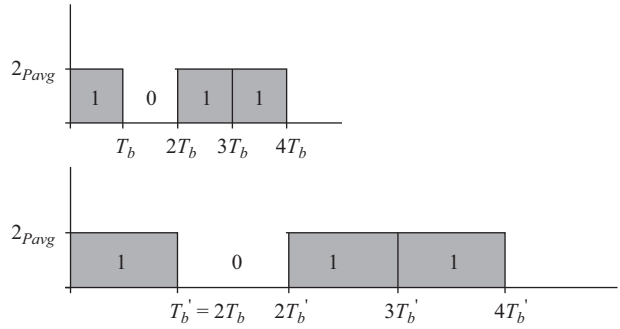

Figure 11.9 Data rate variation by increasing the pulse duration with NRZ-OOK. Top: high data rate (DR), bottom: half of DR

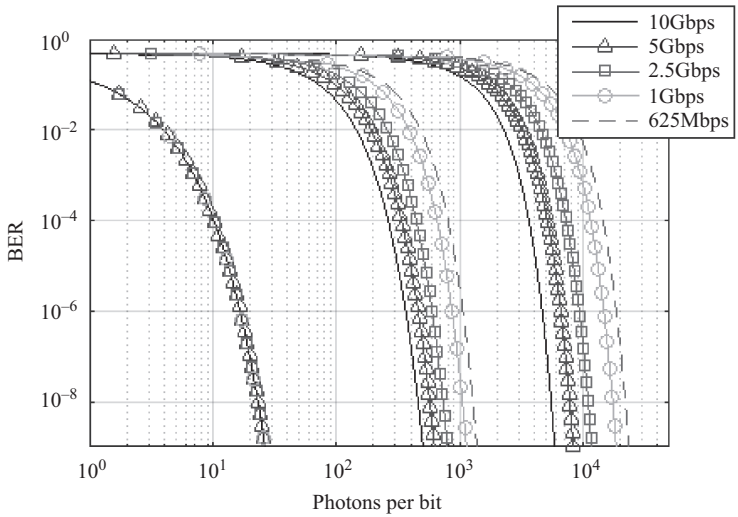

Figure 11.10 BER versus photons per user bit for different data rates and different receiver models (no FEC). Left: SNL, middle: APD, right: PIN

PPM, $M = 2^n$, where n is the number of bits in one symbol. The position of the pulse slot inside its symbol time (unless specified differently) corresponds to the decimal value of the n-bit input data. The symbol duration T_s is divided into L number of slots, each of duration T_b.

Options and effectiveness of data rate variation with different OOK modulation schemes: As explained above, the high channel variability in OLEODL (distance, attenuation and fading) requires variation of the system DR. With the NRZ modulation format, the DR can be lowered by simply increasing the pulse width. Figure 11.9 shows the signal waveform for transmitting NRZ-OOK signals at a high DR (top) and at half that rate (bottom) by doubling the pulse width. Figure 11.10 indicates the

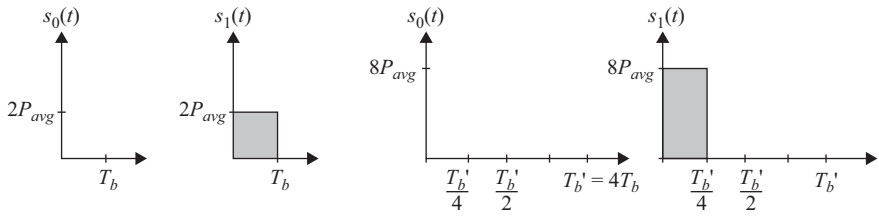

Figure 11.11 Data rate variation by reducing the duty cycle of RZ-OOK. Left: NRZ-OOK at high data rate (DR), right: RZ-OOK with 25% duty cycle and lower data rate (=DR/4)

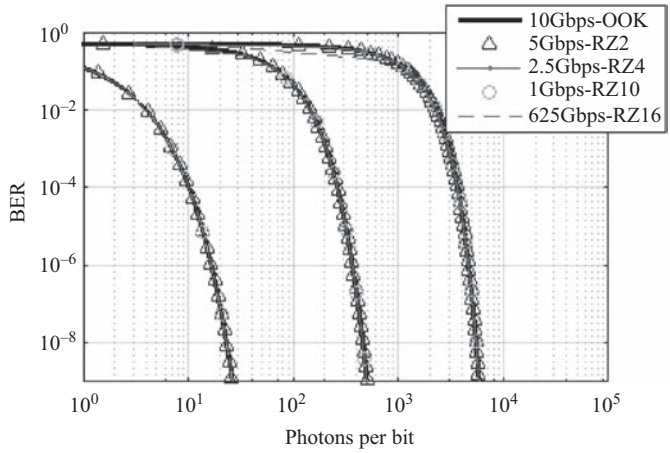

Figure 11.12 BER versus photons per user bit for different data rates and different receiver models. Left: SNL, middle: APD, right: PIN

performance of the system for different DRs for shot-noise-limited (SNL), practical APD and thermal limited positive-intrinsic-negative (PIN) receiver models (see next section for explanations of receiver sensitivity). With an ideal SNL receiver, the system sensitivity in terms of the number of photons per bit (thus energy per bit) required to achieve a certain BER remains constant for different DRs, whereas for APD and PIN, it degrades for higher DRs. For this rate variation scheme, the reception filter low pass in the RFE must be adapted according to channel rate.

With RZ-OOK, the variable pulse duty cycle enables an elegant way to keep the pulse width fixed (and thus also the RFE's reception filter), while the bit length is increased as shown in Figure 11.11. Figure on the left represents bit '0' and '1' at a high DR using NRZ-OOK modulation, while the right one represent bits '0' and '1' at a lower DR (=DR/4) using RZ-OOK modulation with 25% duty cycle. This method introduces longer pauses between the pulses, increasing the pulse amplitude accordingly in a transmitter with constant average power. As a result, system sensitivity in photons per bit for the different DRs stays constant for all types of receivers (SNL, APD, PIN) as seen in Figure 11.12 [44].

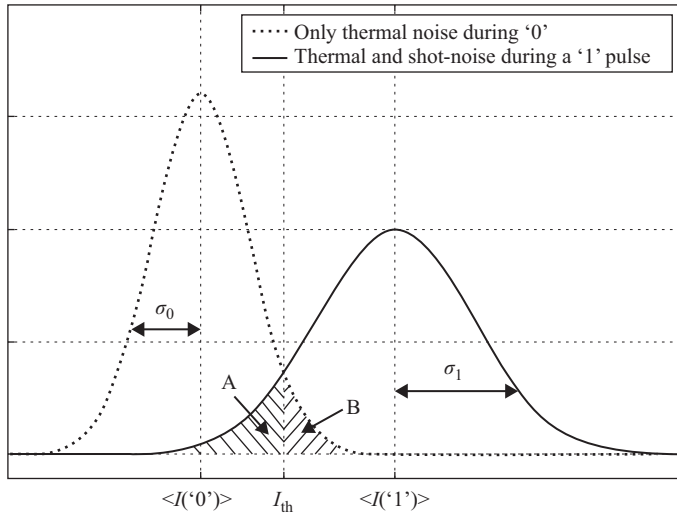

Figure 11.13 Probability distribution of received OOK signal with signal-dependent noise, when '0' (left) and '1' (right) is transmitted in presence of shot and thermal noise. Adopted from Reference [46]

Similarly, PPM also inherently lowers the DR with increasing order, if the pulse length is kept constant; therefore, variable PPM order can be used as a rate variation mechanism. However, the synchronisation effort increases, while the variability is limited due to the logarithmic relation between order and effective DR.

11.2.6 OOK RFE performance and impact on link budget

In OOK receivers, the receiver telescope collects the optical signal, filters the undesired background light and focusses onto the photodetector surface to convert it to an electrical signal current. This signal then has to be detected as pulse or no-pulse by a decision logic at the proper photocurrent threshold (I_{th}), which is derived, e.g. in [45]. If the detected signal is above the threshold, bit '1' is detected, otherwise bit '0' is detected. In addition to the modulated signal, shot noise (possibly signal-dependent) and thermal noise widen its level distribution, which may lead to false detection of the pulse or missed detection. Figure 11.13 shows the Gaussian probability distribution of the signal in addition to noise, and σ_0 and σ_1 are the noise variances, respectively. Areas A and B then indicate the probability of wrong decision leading to bit errors.

Considering all possibilities of errors explained above and assuming each symbol is equally likely, the bit error probability for NRZ-OOK is calculated as

$$BEP = \frac{1}{2} \cdot erfc\left(\frac{\sqrt{SNR}}{\sqrt{2}}\right); \quad \text{where } SNR = \left(\frac{\langle I(\text{'1'})\rangle}{\sigma_0 + \sigma_1}\right)^2 \tag{11.15}$$

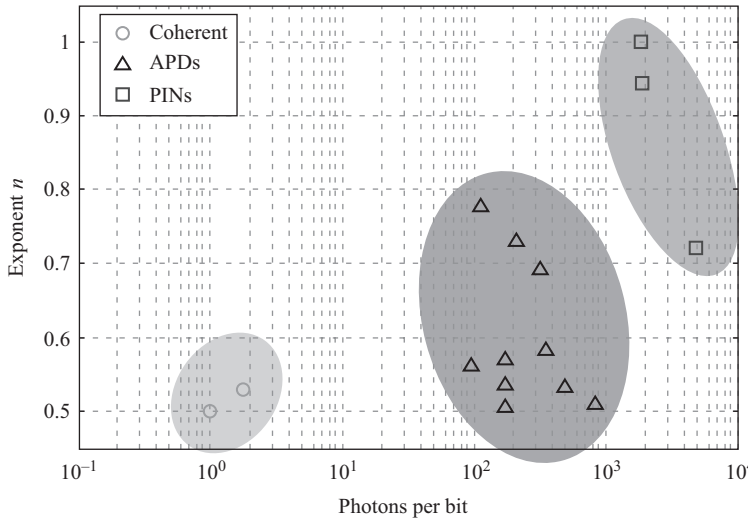

Figure 11.14 Performance ranges of different receiver implementations, derived from measured examples with COTS components. Abscissa indicates required photons per bit for $Q = 2$ (BER = 0.023), and ordinate shows the exponent n of the sensitivity run (measured RFE performances according to [47])

While theoretical derivation of the BER calculation from noise distributions is well understood, practical RFE performance depends on various parameters that often cannot be anticipated, especially in APD receiver realisations which are influenced both by thermal and shot noise. Instead, practically measured RFE performance in terms of BER(P_{Rx}) should be used to model system performance. One method is to use an absolute reference sensitivity (here the received power $P_{Q=2}$ for BER = 2.3% or quality factor $Q = 2$) and an exponent n defining the shape of the sensitivity slope [47].

$$BER = \frac{1}{2} \cdot erfc\left(\frac{Q}{\sqrt{2}}\right) = \frac{1}{2} \cdot erfc\left(\frac{f(\overline{P}_{\mathrm{Rx}})}{\sqrt{2}}\right); \quad Q = \sqrt{SNR_{el}} \tag{11.16}$$

$$Q(\overline{P}_{\mathrm{Rx}}) = 2\left(\frac{\overline{P}_{\mathrm{Rx}}}{\overline{P}_{Q=2}}\right)^{n} \tag{11.17}$$

With this method, various RFE performances can be described sufficiently with their absolute sensitivity in photons per bit for $Q = 2$ and their sensitivity run. Measured examples are given in Figure 11.14. Here, the *coherent* SNL example is a BPSK homodyne receiver, while *APD* (Avalanche Photo Diode) and *PIN* are InGaAs-semiconductor DD receivers.

Channel sensitivities of 100 photons/bit can be achieved with APD-receivers, when the high BER of 2.3% is compensated with according FEC coding.

11.2.7 Error control techniques for Gaussian channels

The transmission of data bits from source to sink is always subject to noise, resulting in a certain probability of erroneous bit detection. To reduce this BER, either the SNR has to be increased (which reduces system efficiency) or techniques to reduce the final BER must be introduced (so-called error control algorithms). This can be ARQ, where bit errors in the received data packets are detected and corresponding repetition of these packets is requested. However, this technique does not apply to simplex links and does not work well for strongly delayed links, as can be the case with satellite downlinks. Alternatively, FEC techniques can be applied. Here, the source data and additional parity data – which are produced from the source data – are transmitted. This additional data allows correction of bit errors experienced during transmission over the noisy channel, and accordingly, the system sensitivity can be increased. Performance parameters of FEC techniques are on the one hand the required overhead (parity-bits) for the code, and on the other, the capability of the code to correct a certain number of erroneous bits in a transmission channel at a certain mean received power.

FEC has been the scope of intense scientific investigation and is indispensable in today's telecommunication field, see basic publications [48–50].

For space links, FEC is considered in-depth in the standardisation documents of CCSDS, e.g. [51]. Figure 11.15 shows a comparison of the basic forward correction codes applied in classical space links. The parameter E_b/N_0 denotes the ratio of received energy per source data bit to the noise power spectral density. This metric allows – amongst others – the comparison of the sensitivity (and thus efficiency) of different modulation formats and coding schemes.

Simple performance relations typically refer to a so-called Gaussian-noise channel, i.e. noise processes follow Gaussian statistics, and single error events are short (fast-fading channel). The picture changes when, e.g. the noise is no longer symmetric around its mean (as in single photon reception channels), or when the error rate changes with slow fading of the received signal. The later requires techniques that span the influence of a codeword over a longer time fraction, as described in the following section.

11.2.8 Interleaving in the atmospheric fading channel

Besides varying the channel symbol rate or symbol modulation order, other variation techniques are based on working directly on the data packets. Such techniques often combine the effective channel rate variation with variable error-control strength (FEC) [52]. Standard coding techniques improve sensitivity in a Gaussian channel but do not specifically compensate the long erasures caused by fading. Spreading the coded data through interleaving over timespans much larger than one fading event therefore helps in achieving an ergodic situation for subsequent FEC. This is of major concern when using small receive antennas which experience high scintillation dynamic, but it gets less important with larger antennas. Interleavers however lead to memory overhead and require additional processing which might be challenging in high DR transmission. Matrix and convolution interleaver are classical interleaver types.

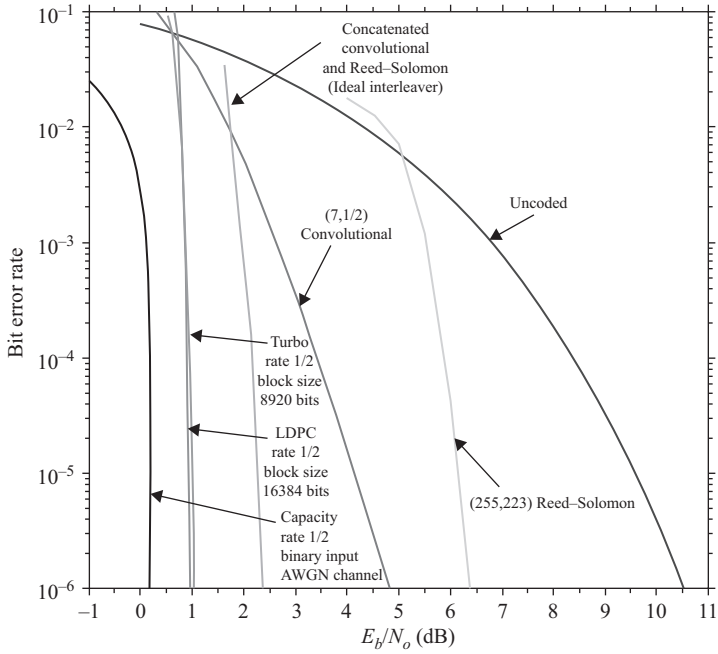

Figure 11.15 Comparison of various FEC coding schemes at different code rates, for a Gaussian (i.e. non-fading) channel and binary phase shift keying modulation. Reprint, with permission, from Figure 3-5 of [51]

In matrix interleaver, the input data is written in rows of a memory configured as a matrix, and then read out column-wise. In a convolutional interleaver, the data is multiplexed into and out of a fixed number of shift registers [53]. Such interleavers can be implemented at bit or codeword level. The basic idea of codeword interleaving is to resequence parts of a long codeword (instead of bits) before transmitting [54]. For optical fading channels, codeword interleavers might be more applicable than extremely large bitwise matrix interleavers (remember that with typical OLEODL DRs with fades in the order of several milliseconds, the memory requirement is in the order of Gigabit). Codeword interleaving can be done in different ways: A single codeword can be simply repeated after a delay longer than the channel correlation time [55]. More efficiently, a codeword may be split into several blocks, each affected from different fading states (so-called block-interleaving). This allows for further sophistication, e.g. sending the data- and parity sections of a systematic FEC-codeword separately [56], or applying a second level of FEC for the blocks. To summarise, the combination of FEC and interleaving works on both aspects – the fading compensation and effective DR variation – and they must be balanced for a specific channel situation with a particular scintillation strength and mean power.

11.3 Hardware

11.3.1 Space hardware

A key component of an optical communication system for LEO satellites in a direct-to-earth application is the satellite payload. The payload on board the satellite has to provide a laser signal, modulate it with the transmission data and keep the tracking of the ground station based on the received beacon laser while the whole payload needs to withstand the environmental influences during launch and in orbit.

Different system designs of the above-mentioned characteristics can be realised. These implementations largely depend on which of the following is selected:

- use of a beacon from the OGS
- active pointing assembly or body pointing of the satellite
- mono-static or bi-static system design.

The most simple and robust system design for an optical communication system on board a satellite is a pure laser source with transmission optics. For this design, the body pointing of the satellite is used together with a rather large divergence of the transmission system so that neither a beacon from the OGS nor a pointing device is required. This simple system design comes with the disadvantage of an inefficient link budget.

Adding a beacon laser on the ground station allows us to increase the efficiency of the system by reducing the transmitter divergence due to the improved tracking of either the body pointing of the satellite or the active pointing device. The use of a beacon from OGS also requires a receive path in the satellite payload in addition to the transmit path.

The tracking signal received from a tracking sensor, which receives the beacon signal from the OGS, can be used either for an improved body pointing of the satellite or for an active pointing stage. Using the body pointing of the satellite reduces the complexity of the optical communication terminal in the satellite but in turn increases the complexity of the attitude control of the satellite. If the attitude control accuracy is sensor-limited, the use of a beacon laser and tracking sensor can improve the attitude control accuracy via a sensor fusion of the satellite attitude sensor with the beacon detector. If the attitude control accuracy is limited by the actuators of the satellite, an active pointing device should be considered in the optical communication terminal. An active pointing device can either be a FPA, which delivers high precision and high speed but only in a small angular range, or a CPA, which covers a large angular range but offers less accuracy and speed – or a combination of both FPA and CPA.

Having both, a receive path for the beacon from OGS as well as a transmit path for the modulated data signal, means that either a mono-static or a bi-static system design needs to be implemented. A bi-static system design is characterised by two different apertures (one for the receive path and one for the transmit path) as shown in Figure 11.16, whereas only one aperture is used for both the receive and the transmit paths in a mono-static system design (compare Figure 11.17).

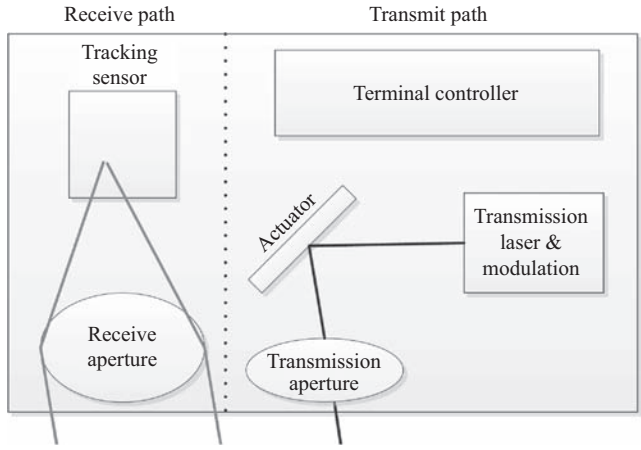

Figure 11.16 Bi-static system design with separate apertures for receive and transmit path

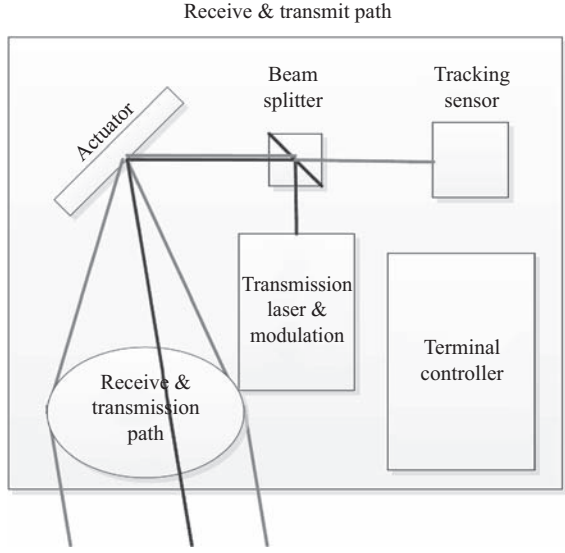

Figure 11.17 Mono-static system design with a combined aperture for receive and transmit path

Both system designs come with advantages and disadvantages. Table 11.6 summarises the advantages and disadvantages of both system designs.

All system designs share the requirement to withstand the environmental influences experienced during the launch of the system as well as during operation in orbit.

Table 11.6 Comparison of advantages and disadvantages of mono-static and bi-static system designs

	Advantages	Disadvantages
Bi-static design	• Simple and robust system design • No separation between transmit and receive path required	• Misalignment might occur due to different apertures • More space required for two separate apertures
Mono-static design	• Highly compact system design • Compensation of misalignment due to same aperture for Rx and Tx	• Separation between Rx and Tx required • More complex system design

While mechanical stress is the primary concern during the launch of the system (due to vibration loads of the launch vehicle), areas of concern during operation in orbit include thermal cycles as well as radiation effects. All of these effects influence the system design in one way or another. While vibration loads mainly have an influence on the mechanical structure and the optical design, radiation affects all electrical and optical components of the terminal. These effects may also lead to a degradation of the component performance on the electrical or optical level as well as a potential complete failure in the case of undetected latch-ups.

For both system designs – but especially for mono-static designs – the wavelengths selection for the receive and transmit path are essential. In the mono-static design, a beam splitter is used to separate the paths. The stray light and back reflections of the transmit path from the optical system need to be suppressed on the tracking sensor with a chromatic beam splitter in combination with filters to avoid self-blinding. The performance of these filters depends on the wavelength gap between receive and transmit signals. In addition to the separation of the receive and transmit path, the presence of absorption lines in the atmospheric spectrum plays a major role in the wavelength selection (compare Figure 11.7). Figure 11.18 shows exemplary band plans with different options for uplink beacon and downlink. For the selection of wavelengths, defining a spectral range free from absorption lines is a major driver. The absorption lines (resulting from water vapour and other molecules in the atmosphere) occur throughout the entire optical C- and L-bands and influence the transmittance of certain wavelengths, resulting in an attenuation that increases with lowering elevation. The band plan shows a favourable downlink wavelength range from 1,545 to 1,565 nm for multiple downlink channels to be selected within this window. Based on the wavelength gap between receive and transmit paths, which is ideally not less than 20 nm due to manufacturing complexity of the wavelength separation components, three options for beacon wavelengths are found: 1,064, 1,530 and 1,590 nm. Option 1

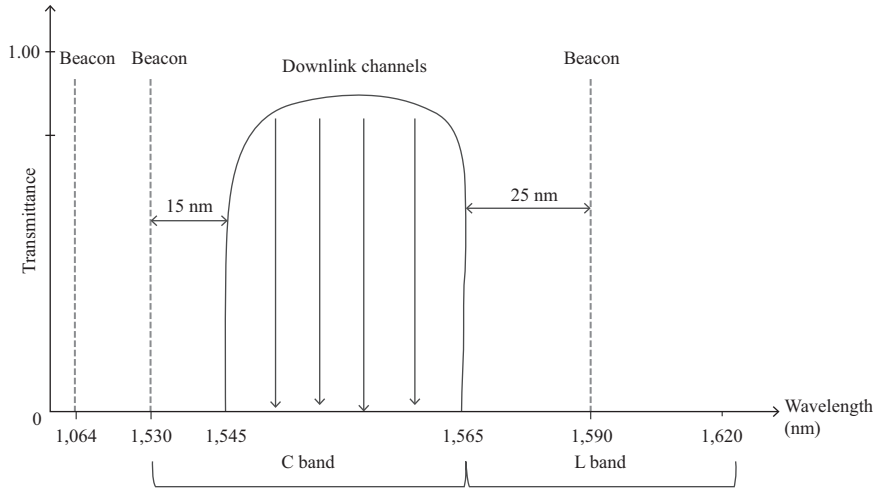

Figure 11.18 Band plan examples for beacon as well as transmission wavelengths

with 1,064 nm comes with the advantage of a large wavelength gap between receive and transmit paths together with a good availability of components but raises challenges regarding laser safety. Option 2 at 1,530 nm is the lowest wavelength within the optical C-band and allows to have both downlink and beacon in the same optical band, and the availability of components is good due to the use in fibre communication. However, this option comes with the disadvantage of a limited wavelength gap or reduced bandwidth for the downlink channels if the wavelength gap is increased, together with a high presence of absorption lines in this area and accordingly higher demand on beacon wavelength control. Option 3 at 1,590 nm (lower end of the optical L-band) allows for a wavelength gap of more than 25 nm while allowing to use the full downlink window in combination with lower presence of absorption lines in this area. Based on the requirements and characteristics of the scenario, an optimised beacon and downlink wavelength combination can be selected.

11.3.2 Ground hardware

LEO downlinks need an OGS as a receiver terminal. Setups with Cassegrain, Ritchey–Chretien and similar telescope configurations are common. Here, the data and tracking receivers would be installed in the Cassegrain focus or a conjugated plane. More experimental stations may deploy a Coudé focus. Then, more complex and experimental receivers and sensors can be set up on the Coudé focus optical bench. Most currently used ground telescopes have primary mirror diameters of about 20 cm–1.5 m, depending on the actual link distance and transmit antenna gain. A diameter of 40–60 cm is usually sufficient for receivers in LEO ground communications. The application of a wavefront correction system may also be needed if fibre coupling

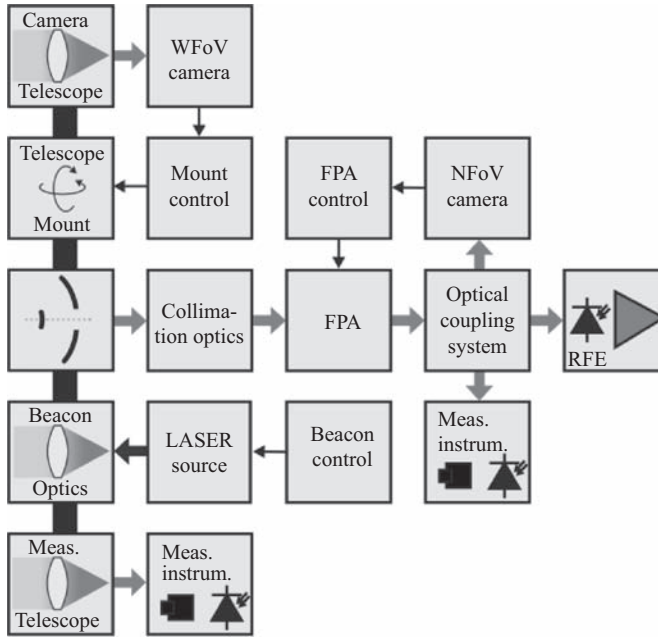

Figure 11.19 Basic block diagram of the OGS-OP optical system. The black bar indicates the mechanical connection of the functional blocks [57]

is necessary. The corresponding adaptive optics system is then often set up on a Coudé-bench.

To date, systems are mainly built for experiments and demonstrations, a list of known ground station installations is given in Table 11.2. Figure 11.19 shows exemplary the basic block diagram for DLR's Optical Ground Station Oberpfaffenhofen (OGS-OP). The black bar shall indicate that these elements are mechanically joint. The control software is steering the telescope mount to point towards the satellite. A wide field of view camera is installed to provide coarse optical tracking. A beacon laser telescope is co-aligned for the PAT process. Optional measurement telescopes are installed alongside for channel measurements. Behind the telescope, collimation optics together with the telescope form an afocal system. The FPA stabilises the beam to ensure that residual tracking errors are kept to a minimum. An optical coupling system (free-space) distributes beams to the near field of view camera for fine tracking, to the measurement instruments and to the data RFE.

The most important system aspects of a ground station are the antenna gain, the accompanying aperture averaging of scintillation, the tracking accuracy and beacon systems. The antenna gain is governed by the size of the primary mirror as described by (11.6). An increase in size not only increases the antenna gain but also reduces fading events due to the lower power scintillation seen on the data receiver. The aperture

averaging factor *AAF*, i.e. the relation between scintillation with finite aperture size $\sigma_I^2(D)$ to infinitesimal small aperture size $\sigma_I^2(0)$, is a measure of how effectively a finite aperture can suppress fading events.

Another effect of aperture averaging is the transformation of intensity statistics from gamma–gamma or exponential distributions to lognormal distributions, i.e. from distributions in strong fluctuations to distributions in weak fluctuation conditions. See [58] for details on the transformation from intensity statistics to received-power statistics through aperture averaging under varying link elevation.

Tracking systems in the OGSs can be designed with almost arbitrarily high complexity. The minimum tracking capability requirement is to steer the whole telescope towards the satellite and keep line of sight. If this can be achieved with sufficient accuracy, no second stage tracking system, such as a fine tracking system for beam stabilisation or fibre coupling needs to be used. An example for a system with a one stage tracking system is DLR's transportable optical ground station (TOGS). This station achieved a residual peak tracking error in the demanding aircraft ground scenario of well below 100 μrad and is therefore precise enough to keep the signal spot on the RFE with field of view of 170 μrad. DLR's TOGS is also equipped with an uplink beacon laser system according to the band plan in Figure 11.18. Besides the wavelength of the beacon system, the optical output power, modulation frequency as well as divergence angle are to be considered in the system design.

11.4 Summary and outlook

Within this chapter, high-speed optical satellite data downlinks have been reviewed and the key characteristics of this application scenario have been described. The excellent properties of optical links, especially the high data rate, license free operation and favourable SWaP (size, weight and power) provide a game-changing technological alternative to RF-links for Earth observation satellite operators. Despite some drawbacks of the technology, industries and research organisations around the world are now developing optical communication systems that are suitable for downlink applications, demonstrating the potential of the technology and underlining its future importance for various applications.

Due to the fact that optical space-to-ground links suffer from limited availability due to clouds, OGS networks enable OGS diversity to ensure a reliable operation scenario. The availability of space-to-ground links is subject of current research [33,59]. It has been shown that, with a suitable OGS network design, the issue of limited link availability vanishes when a suitable buffer memory size is employed on the satellite to bridge weather-induced unavailability of OGSs. OGS networks are a key requirement for the future use of optical satellite downlinks and need to be established and operated.

A field which is gaining increasing attention is the installation of so-called LEO-Mega-Constellations for low-delay global communications, with orbital altitudes in the order of 1,000 km. These systems are not meant to serve for the transmission of remote sensing or Earth observation data to the ground. Rather, they are designed to

enable Internet access in areas with limited terrestrial capabilities, as e.g. in developing countries. Several particularly rural regions in Europe also could benefit from Internet access through satellites. To avoid interference with terrestrial RF-communications and enable high DRs, the internetworking of these constellations will be favourably done with symmetric optical data links. Their link distances are similar to those of OLEODL, and accordingly terminal hardware will work in a likewise way. Thus, developments of optical LEO communications may see two use cases, allowing even compatible link technology between these transmission scenarios.

References

[1] T. Tolker-Nielsen, J-C. Guillen, "SILEX the first European optical communication terminal in orbit", ESA Bulletin 96, Nov. 1998.

[2] H. Zech, F. Heine, D. Tröndle, *et al.*, "LCT for EDRS: LEO to GEO optical communications at 1,8 Gbps between Alphasat and Sentinel 1a", Proc. SPIE 9647, 2015.

[3] Y. Chishiki, S. Yamakawa, Y. Takano, Y. Miyamoto, T. Araki, H. Kohata, "Overview of optical data relay system in JAXA", Proc. SPIE 9739, 2016.

[4] E. Luzhanskiy, B. Edwards, D. Israel, *et al.*, "Overview and status of the laser communication relay demonstration", Proc. SPIE 9739, 2016.

[5] D.M. Cornwell, "NASA's optical communications program for 2017 and beyond", IEEE International Conference on Space Optical Systems and Applications (ICSOS) 2017, 2017.

[6] A. Biswas, J.M. Kovalik, M. Srinivasan, *et al.*, "Deep space laser communications", Proc. SPIE 9739, 2016.

[7] ESA, RUAG, DLR, *et al.*, "DOCOMAS – Deep Space Optical Communications Architecture Study, Executive Summary", 2016, downloaded 25.Sep. 2017.

[8] D. Giggenbach, E. Lutz, J. Poliak, R. Mata-Calvo, C. Fuchs, "A high-throughput satellite system for serving whole Europe with fast internet service, employing optical feeder links", ITG-Conference "Breitbandversorgung in Deutschland", Berlin, Apr. 20–21, 2015.

[9] T. Jono, Y. Takayama, N. Kura, *et al.*, "OICETS on-orbit laser communication experiments", Proc. SPIE, 6105, 2006.

[10] T. Jono, Y. Takayama, N. Perlot, *et al.*, "Report on DLR-JAXA Joint Experiment: The Kirari Optical Downlink to Oberpfaffenhofen (KIODO)", JAXA and DLR, ISSN 1349-1121, 2007.

[11] D. Giggenbach, F. Moll, N. Perlot, "Optical communication experiments at DLR", NICT Journal Special Issue on the Optical Inter-orbit Communications Engineering Test Satellite (OICETS), vol. 59, pp. 125–134, 2012.

[12] A. Carrasco-Casado, H. Takenaka, D. Kolev, *et al.*, "LEO-to-ground optical communications using SOTA (Small Optical TrAnsponder) – Payload verification results and experiments on space quantum communications", Acta Astronautica, vol. 139, pp. 377–384, 2017.

[13] A. Biswas, B, Oaida, K. Andrews, *et al.*, "Optical Payload for Lasercomm Science (OPALS) link validation during operations from the ISS", SPIE Proceedings 9354, 2015.

[14] F. Moll, D. Kolev, M. Abrahamson, C. Schmidt, R. Mata Calvo, C. Fuchs, "LEO-ground scintillation measurements with the Optical Ground Station Oberpfaffenhofen and SOTA/OPALS space terminals", Proceedings of SPIE 9991 (Advanced Free-Space Optical Communication Techniques and Applications II), 2016, 999102-1–999102-8.

[15] C. Schmidt, M. Brechtelsbauer, F. Rein, C. Fuchs, "OSIRIS payload for DLR's BiROS satellite", International Conference on Space Optical Systems and Applications – ICSOS, Kobe, Japan, 2014.

[16] D. Giggenbach, A. Shrestha, C. Fuchs, C. Schmidt, F. Moll, "System aspects of optical LEO-to-ground links", International Conference on Space Optics, Biarritz, France, Oct. 2016.

[17] M. Toyoshima, K. Takizawa, T. Kuri, *et al.*, "Ground-to-OICETS laser communication experiments", Proc. of SPIE, 6304B, 2006, 1–8.

[18] N. Perlot, M. Knapek, D. Giggenbach, *et al.*, "Results of the optical downlink experiment KIODO from OICETS satellite to optical ground station Oberpfaffenhofen (OGS-OP)", Proc. of SPIE 6457, 2007.

[19] M.R. Garcia-Talavera, Z. Sodnik, P. Lopez, A. Alonso, T. Viera, G. Oppenhauser, "Preliminary results of the in-orbit test of ARTEMIS with the optical ground station", Proc. SPIE 4635, 2002.

[20] H. Takenaka, Y. Koyama, D. Kolev, *et al.*, "In-orbit verification of small optical transponder (SOTA) – Evaluation of satellite-to-ground laser communication links", Proc. of SPIE 9739, 2016.

[21] C. Schmidt, M. Brechtelsbauer, F. Rein, C. Fuchs, "OSIRIS payload for DLR's BiROS satellite", International Conference on Space Optical Systems and Applications 2014. ICSOS 2014, Kobe, Japan, 7.–9. Mai 2014.

[22] B. Smutny, H. Kaempfner, G. Muehlnikel, *et al.*, "5.6 Gbps optical intersatellite communication link", Proc. of SPIE 7199, 2009.

[23] M. Toyoshima, T. Kuri, W. Klaus, *et al.*, "4-2 Overview of the laser communication system for the NICT optical ground station and laser communication experiments in ground-to-satellite links", Special issue of the NICT Journal, vol. 59, no. 1/2, pp. 53–75, 2012.

[24] Z. Sodnik, B. Furch, H. Lutz, "The ESA optical ground station – Ten years since first light", ESA Bulletin 132, Nov. 2007.

[25] K. Saucke, C. Seiter, F. Heine, *et al.*, "The Tesat transportable adaptive optical ground station", Proc. of SPIE 9739, 2016.

[26] K. Wilson, N. Page, J. Wu, M. Srinivasan, "The JPL optical communications telescope laboratory test bed for the future optical deep space network", IPN Progress Report 42-153, 2003.

[27] D.-H. Pung, E. Samain, N. Maurice, *et al.*, "Telecom & scintillation first data analysis for DOMINO – laser communication between SOTA onboard Socrates satellite and MEO OGS", Space Optical Systems and Applications (ICSOS), New Orleans, 2015.

[28] C. Schmidt, C. Fuchs, "The OSIRIS program – First results and outlook", IEEE International Conference on Space Optical Systems and Applications (ICSOS) 2017, 2017.
[29] T. Dreischer, B. Thieme, K. Buchheim, "Functional system verification of the OPTEL-μ laser downlink system for small satellites in LEO", International Conference on Space Optical Systems and Applications (ICSOS) 2014, 2014.
[30] T. Shih, O. Guldner, F. Khatri, *et al.*, "A modular, agile, scalable optical terminal architecture for space communications", IEEE International Conference on Space Optical Systems and Applications (ICSOS) 2017, 2017.
[31] B.L. Edwards, "An update on the CCSDS optical communications working group", IEEE International Conference on Space Optical Systems and Applications (ICSOS) 2017, 2017.
[32] D. Giggenbach, F. Moll, C. Fuchs, T. de Cola, R. Mata-Calvo, "Space communications protocols for future optical satellite-downlinks", 62nd International Astronautical Congress, 3.Okt–7.Okt 2011, Cape Town, South Africa, 2011.
[33] C. Fuchs, S. Poulenard, N. Perlot, J. Riedi, J. Perdigues, "Optimization and throughput estimation of optical ground networks for LEO-downlinks, GEO-feeder links and GEO-relays", Proc. SPIE 10096, Feb. 24, 2017.
[34] L.C. Andrews, R.L. Phillips, "Laser Beam Propagation through Random Media, 2nd Edition", SPIE-Press, Bellingham, WA, 2005.
[35] N. Perlot, T. De Cola, "Throughput maximization of optical LEO-ground links", Free-Space Laser Comm. Technologies XXIV, San Francisco, USA, 2012.
[36] F. Moll, M. Knapek, "Wavelength selection criteria and link availability due to cloud coverage statistics and attenuation affecting satellite, aerial, and downlink scenarios", Proceedings of SPIE 6709, 2007.
[37] I.E. Gordon, L.S. Rothman, C. Hill, *et al.*, "The HITRAN2016 molecular spectroscopic database", Journal of Quantitative Spectroscopy and Radiative Transfer, vol. 203, pp. 3–69, Dec. 2017.
[38] H. Hemmati, M. Toyoshima, R.G. Marshalek, *et al.* (Ed.) Near-Earth Laser Communications, CRC Press, Boca Raton, FL, 2009.
[39] W.R. Leeb, "Degradation of signal to noise ratio in optical free space data links due to background illumination", Applied Optics, vol. 28, pp. 3443–3449, 1989.
[40] D. Giggenbach, H. Henniger, "Fading-loss assessment in atmospheric free-space optical communication links with on-off keying", Optical Engineering, vol. 47, pp. 046001-1–046001-6, 2008.
[41] S.G. Lambert, W. Casey, Laser Communications in Space, Artech House, Norwood, MA, 1995.
[42] M.D. Eisaman, J. Fan, A. Migdall, S.V. Polyakov, "Single-photon sources and detectors", Review of Scientific Instruments, vol. 82, 2011.
[43] Z. Ghassemlooy, W. Popoola, S. Rajbhandari, "Optical Wireless Communications: System and Channel Modelling with MATLAB", 2013.
[44] A. Shrestha, D. Giggenbach, "Variable data rate for Optical Low-Earth-Orbit (LEO) Downlinks", ITG-Fachbericht 264: Photonische Netze, 12–13 May 2016, Leipzig, Germany, 2016.

[45] G.P. Agrawal, "Fiber-Optic Communication Systems, 3rd Edition", John Wiley & Sons, New York, 2002.
[46] D. Giggenbach, "Optimierung der optischen Freiraumkommunikation durch die turbulente Atmosphäre – Focal Array Receiver", PhD. Thesis, University of German Federal Armed Forces, Munich, 2004.
[47] D. Giggenbach, R. Mata-Calvo, "Sensitivity Modelling of Binary Optical Receivers", Applied Optics, vol. 54, no. 28, Oct. 2015.
[48] C.E. Shannon. "A Mathematical Theory of Communication", Bell System Technical Journal, vol. 27, no. 3, pp. 379–423, Jul. 1948.
[49] B. Sklar, "Digital Communications: Fundamentals and Applications, 2nd Edition", Prentice-Hall, Upper Saddle River, NJ, 2001.
[50] S. Lin, D.J. Costello, "Error Control Coding", Prentice Hall, Upper Saddle River, NJ, 2004.
[51] "TM Synchronization and Channel Coding – Summary and Rationale", CCSDS-130.1-G-2, Consultative Committee for Space Data Systems, Washington, DC, Nov. 2012.
[52] G. Gho, L. Klak, J.M. Kahn, "Rate-adaptive coding for optical fiber transmission systems", Journal of Lightwave Technology, vol. 29, no. 2, 2011.
[53] G.D. Forney, "Burst-correcting codes for the classic bursty channel", IEEE Transactions of Communications Technology, Vol. 19, no. 1971, pp. 772–781, 1971.
[54] A. Botta, A. Pescape, "IP packet interleaving: bridging the gap between theory and practice", IEEE, 2011.
[55] A. Shrestha, D. Giggenbach, N. Hanik, "Delayed frame repetition for free space optical communication (FSO) channel", ITG-Fachbericht 272: Photonische Netze, 11–12 May 2017, Leipzig, Germany, 2017.
[56] F. Xu, A. Khalighi, P. Caussé, S. Bourennane, "Channel coding and time-diversity for optical wireless links", Optics Express, vol. 17, no. 2, pp. 872, 2009.
[57] F. Moll, A. Shrestha, C. Fuchs, "Ground stations for aeronautical and space laser communications at German Aerospace Center", Proc. of SPIE 9647, 2015.
[58] D. Giggenbach, F. Moll, "Scintillation loss in optical low Earth orbit data downlinks with avalanche photodiode receivers", IEEE-Xplore, International Conference on Space Optical Systems 2017 (ICSOS), 13.–16. Nov. 2017, Naha, Japan, 2017.
[59] S. Poulenard, A. Mège, C. Fuchs, N. Perlot, J. Riedi, and J. Perdigues, "Digital optical feeder links system for broadband geostationary satellite", Proc. of SPIE, 10096, 2017, pp. 1009614–1.